Chapter

Emergence of Raman Peaks Due to Septic Nonlinearity in Noninstantaneous Kerr Media

Michel-Rostand Soumo Tchio, Saïdou Abdoulkary and Alidou Mohamadou

Abstract

We analyze the modulation instability induced by cross-phase modulation of two co-propagating optical beams in nonlinear fiber with the effect of higher-order dispersion and septic nonlinearity. We investigate in detail the effect of relaxation nonlinear response to the gain spectrum both in normal group velocity dispersion (GVD) and anomalous dispersion regime. We show that the walk-off, the relaxation nonlinear response time as well as the higher-order process particularly influence the generation of the modulation instability gain. Our results shows that the emerging Raman peaks is observable both in the case of weak dispersion and in a higher-order dispersion for mixed GVD regime with slow response time. These Raman peaks are shifted toward higher frequencies with the decrease of their magnitude, when the walk-off increases.

Keywords: septic nonlinearity, higher-order dispersions, walk-off effects, delay response time, cross-phase modulation

1. Introduction

The generation of a wave train is a preoccupying subject in the realm of nonlinear science. This is mainly due to two effects: nonlinearity and dispersion. These two notions are essential in the propagation of the wave over long distances and the optical pulse resulting from this interaction gives rise to an optical soliton. The dynamic evolution of nonlinear pulses in nonlinear optical systems can be modeled by the well known nonlinear Schrödinger (NLS) equation which represents the lowest-order nontrivial condition describing the propagation process [1]. The co-propagation of two nonlinear waves in nonlinear optical Kerr media under a slowly varying amplitude approximation is made by using extensions of the NLS equation, whose analytical results provide the dispersion relation, the unstable conditions, as well as the gain spectra. This extension of NLS equation can take into account a large variety of physical properties such as higher-orders dispersion (like third-order dispersion (TOD) and fourth-order dispersion (FOD)) [2–9]; multiple optical beams [10]; negative index material [11]; saturable nonlinearity [12]; and non-instantaneous nonlinear response [13]. Third-order dispersion is used to describe the proprieties of ultrashort pulses in the subpicosecond to femtosecond domain. Usually in nonlinear optic, Kerr nonlinearity is used to compensate the dispersion effects leading to the formation of soliton. Due to this property, focusing Kerr-type media promote the stable propagation of bright solitons [14]. Despite this, the diffraction effect is not enough to balance the self-focusing in focusing quintic nonlinear media and therefore the pulse undergoes critical collapse [15]. Thus, higher-order nonlinearities (HON) play an important role in the description and the propagation of the pulses in Kerr media. Consequently, the extension of NLS equation can also take into account the effect of HON. Reyna et al. [16–18] have experimentally and numerically investigated the nonlinearity management and spatial modulation instability for cubic, quintic, and septic nonlinearity for optical beams propagation in metal-dielectric nanocomposites.

The study of the propagation of an intense optical beams through a nonlinear and dispersive media may lead to fascinating effects such as exponential growth of amplitude due to modulation in amplitude and frequency. This effect is called modulation instability (MI). Modulation instability is a fundamental phenomenon firstly detected in hydrodynamic systems [19] and appears in most nonlinear wave systems. In nonlinear Kerr media such as optical fiber, MI results from the interaction between the nonlinear and dispersive effects [20] characterized by the instability undergone by a continuous wave (cw) or quasi-cw when it propagates inside a nonlinear dispersive system with low noise [21]. Modulation instability has been studied for waves in fluids dynamics [22], plasmas physic [23], dielectric media [24], electrodynamics [25], and atomic Bose-Einstein condensates [26, 27] and was first analyzed theoretically in glass fiber by Hasegawa and Brinkman [28] in 1984 to study the generation of ultrashort optical beams. This phenomenon is generally studied in the anomalous dispersion regime, but it can also be observed in normal dispersion regime when the pumping is carried out close to the zero dispersion subject to certain conditions on the higher order dispersion (HOD) coefficients [29, 30]. Cavalcanti et al. [31] predicted the possibility of MI to occur even in normal group velocity dispersion regime due to the negative values of fourth-order dispersion (FOD). The effects of FOD was also been investigated by many authors who show their inclusion leads to generation of new spectral window. Tchofo et al. have analytically and numerically investigated the behavior of MI under the combined effects of HOD and delayed Raman response [5, 6]. In Ref. [7], the authors shown that FOD shifts the MI peak gain to the higher frequency side and also increases the instability region. Nithyanandan et al. [8] analyzed that the cumulative effect of HOD and walk-off brings new characteristic spectral bands at a definite frequency window.

Wang et al. have shown in their work that the distribution of speed of system flow and the speed of sound determining the occurrence of the sonic horizon is in agreement with the corresponding quantities obtained from a pure numerical evaluation for quantum system incorporating septic nonlinearity modeled by NLS equation [32]. An essential manifestation of the intensity dependence of the refractive index in nonlinear optical media rises through self-phase modulation (SPM) [33], which leads to spectral spreading of optical pulses. It is well known that the co-propagation of two optical waves in nonlinear Kerr media is coupled due to refractive index of the media through the nonlinear phenomenon called cross-phase modulation (XPM) [29, 34].

In this paper, we study the MI in non-instantaneous Kerr media with cubic-quintic-septic nonlinearity, described by a system of two-coupled NLS equation. We mainly focus on revealing the contribution of group velocity mismatch δ, relaxing Kerr nonlinearity, delay response time, cross-phase modulation, and higher-order terms. Analyzing the interplay between instantaneous and non-instantaneous Kerr response for the case of the beams is experiencing normal GVD, and the order beams undergo anomalous GVD. In Section 2, we present the model equation and the linear stability analysis approach; Section 3 features the investigation of MI in the case of weak dispersion regime with the effects of HON. Section 4 is devoted to the analysis of MI gain spectrum by considering the relation between higher-order effects and delay response time. And finally, the conclusion is given in Section 5.

2. Model equations and linear stability analysis

The optical electromagnetic field propagations are described, under a slowly varying amplitude approximation by a coupled nonlinear Schrödinger equation (CNLSE) with higher order dispersion [8] in a single-mode optical Kerr media where higher-order nonlinearities [16] are taken into account. These equations result from two optical beams at different frequencies and the same polarizations where time-dependent nonlinear response is incorporated in the system. The governing systems are read as:

$$i\left(\frac{\partial A_1}{\partial z}+\frac{\delta}{2}\frac{\partial A_1}{\partial t}\right)=\frac{\beta_{21}}{2}\frac{\partial^2 A_1}{\partial t^2}+i\frac{\beta_{31}}{6}\frac{\partial^3 A_1}{\partial t^3}-\frac{\beta_{41}}{24}\frac{\partial^4 A_1}{\partial t^4}-\gamma_1 N_1 A_1, \tag{1}$$

$$i\left(\frac{\partial A_2}{\partial z}-\frac{\delta}{2}\frac{\partial A_2}{\partial t}\right)=\frac{\beta_{22}}{2}\frac{\partial^2 A_2}{\partial t^2}+i\frac{\beta_{32}}{6}\frac{\partial^3 A_2}{\partial t^3}-\frac{\beta_{42}}{24}\frac{\partial^4 A_2}{\partial t^4}-\gamma_2 N_2 A_2. \tag{2}$$

$$\begin{aligned}\frac{\partial N_1}{\partial t}=\frac{1}{\tau}[&-N_1+\kappa_1\left(|A_1|^2+2|A_2|^2\right)+\kappa_2\left(|A_1|^4+6|A_1|^2|A_2|^2+3|A_2|^4\right)\\&+\kappa_3\left(|A_1|^6+18|A_1|^2|A_2|^4+12|A_1|^4|A_2|^2+4|A_2|^6\right)],\end{aligned} \tag{3}$$

$$\begin{aligned}\frac{\partial N_2}{\partial t}=\frac{1}{\tau}[&-N_2+\kappa_4\left(2|A_1|^2+|A_2|^2\right)+\kappa_5\left(3|A_1|^4+6|A_1|^2|A_2|^2+|A_2|^4\right)\\&+\kappa_6\left(4|A_1|^6+12|A_1|^2|A_2|^4+18|A_1|^4|A_2|^2+|A_2|^6\right)]\end{aligned} \tag{4}$$

(κ_1, κ_4), (κ_2, κ_5), and (κ_3, κ_6) are respectively cubic, quintic, and septic nonlinearities parameters.

The nonlinear Kerr parameters γ_i can be expressed as $\gamma_1 = \gamma_2 = n_2/n_0$, the cubic parameters κ_i defined by $\kappa_1 = \kappa_4 = 1$ are control parameters and the quintic-septic parameters can be given, respectively, by $\kappa_2 = \kappa_5 = n_4/n_2$ and $\kappa_3 = \kappa_6 = n_6/n_2$. Where $k = 2\pi n_0/\lambda$ with λ being the wavelength of the laser pump, n_0 is the linear refractive index of the host medium, n_2, n_4, and n_6 are, respectively, the characteristic nonlinear coefficients of the material related to third, fifth and seventh-order susceptibility.

Reyna et al. [16] have proposed this class of HON to study the spatial phase modulation induced by quintic and septic nonlinearities for optical beams propagation in metal colloids, where septic nonlinearity arises from the development up to seventh-order susceptibility of theoretical treatment of Maxwell-Garnett model. Quintic nonlinearity has been considered by Kumar [35] to show the influence of spatial delay on the modulational instability in a composite system with a controllable nonlinearity.

We extend the previous works on MI taking into account the CNLS with higher-order effects and using the linear stability approach. Therefore, we study the stability of the steady-state solution of the above dynamical equations against the small harmonic perturbations; the steady-state solution of the continuous wave (cw) is obtained by setting the time derivative in Eqs. (1)–(4) to zero. This leads the exacts solution in the form: $A_1 = A_1^0 e^{\left[i\gamma_1 N_1^{cw} z\right]}$, $A_2 = A_2^0 e^{\left[i\gamma_2 N_2^{cw} z\right]}$, where N_1^{cw} and N_2^{cw} reads as: $N_1^{cw} = \kappa_1\left(\left|A_1^0\right|^2 + 2\left|A_2^0\right|^2\right) + \kappa_2\left(\left|A_1^0\right|^4 + 6\left|A_1^0\right|^2\left|A_2^0\right|^2 + 3\left|A_2^0\right|^4\right) + \kappa_3\left(\left|A_1^0\right|^6 + 18\left|A_1^0\right|^2\left|A_2^0\right|^4 + 12\left|A_2^0\right|^4\left|A_2^0\right|^2 + 4\left|A_2^0\right|^6\right)$, $N_1^{cw} = \kappa_4\left(2\left|A_1^0\right|^2 + \left|A_2^0\right|^2\right) + \kappa_5\left(3\left|A_1^0\right|^4 + 6\left|A_1^0\right|^2\left|A_2^0\right|^2 + \left|A_2^0\right|^4\right) + \kappa_6\left(4\left|A_1^0\right|^6 + 12\left|A_1^0\right|^2\left|A_2^0\right|^4 + 18\left|A_1^0\right|^4\left|A_2^0\right|^2 + \left|A_2^0\right|^6\right)$ and corresponding to nonlinear phase shift. The dynamic of the system is studied by taking into account the small perturbation using the linear stability analysis theory. Hence, we impose a slight modulation on plane wave as:

$$A_1 = \left[A_1^0 + a_1(z,t)\right]e^{\left[i\gamma_1 N_1^{cw} z\right]}, \tag{5}$$

$$A_2 = \left[A_2^0 + a_2(z,t)\right]e^{\left[i\gamma_2 N_2^{cw} z\right]}. \tag{6}$$

and

$$N_1 = n_1(z,t) + N_1^{cw}, \tag{7}$$

$$N_2 = n_2(z,t) + N_2^{cw}. \tag{8}$$

where $a_j(z,t)$ are the complex functions and assumed to be small in comparison with the amplitude of the carrier wave ($\left|a_j(z,t)\right|^2 \ll \left|A_j^0\right|^2$), and $n_j(z,t)$ are a small deviation from the stationary solution of the nonlinear index. Then inserting Eqs. (5)–(8) in Eqs. (1)–(4), we obtain a set of coupled complex linearized nonlinear Schrödinger equations satisfying the perturbation $a_j(z,t)$ and $n_j(z,t)$ as follows:

$$i\frac{\partial a_1}{\partial z} + \frac{i}{v_{g1}}\frac{\partial a_1}{\partial t} = \frac{1}{2}\beta_{21}\frac{\partial^2 a_1}{\partial t^2} + i\frac{1}{6}\beta_{31}\frac{\partial^3 a_1}{\partial t^3} - \frac{1}{24}\beta_{41}\frac{\partial^4 a_1}{\partial t^4} - \gamma_1 n_1 A_1^0, \tag{9}$$

$$i\frac{\partial a_2}{\partial z} + \frac{i}{v_{g2}}\frac{\partial a_2}{\partial t} = \frac{1}{2}\beta_{22}\frac{\partial^2 a_2}{\partial t^2} + i\frac{1}{6}\beta_{32}\frac{\partial^3 a_2}{\partial t^3} - \frac{1}{24}\beta_{42}\frac{\partial^4 a_2}{\partial t^4} - \gamma_2 n_2 A_2^0. \tag{10}$$

$$\begin{aligned}\frac{\partial n_1}{\partial t} = \frac{1}{\tau}\Big[&-n_1 + \kappa_1\left[A_1^0\left(a_1 + a_1^*\right) + 2A_2^0\left(a_2 + a_2^*\right)\right] + \kappa_2\left[2\left|A_1^0\right|^3\left(a_1 + a_1^*\right)\right.\\ &\left.+6\left|A_1^0\right|^2 A_2^0\left(a_2 + a_2^*\right) + 6\left|A_2^0\right|^2 A_1^0\left(a_1 + a_1^*\right) + 6\left|A_2^0\right|^3\left(a_2 + a_2^*\right)\right] + X_1\Big],\end{aligned} \tag{11}$$

$$\begin{aligned}\frac{\partial n_2}{\partial t} = \frac{1}{\tau}\Big[&-n_2 + \kappa_4\left[2A_1^0\left(a_1 + a_1^*\right) + A_2^0\left(a_2 + a_2^*\right)\right] + \kappa_5\left[6\left|A_1^0\right|^3\left(a_1 + a_1^*\right)\right.\\ &\left.+6\left|A_1^0\right|^2 A_2^0\left(a_2 + a_2^*\right) + 6\left|A_2^0\right|^2 A_1^0\left(a_1 + a_1^*\right) + 2\left|A_2^0\right|^3\left(a_2 + a_2^*\right)\right] + X_2\Big]\end{aligned} \tag{12}$$

with X_1 and X_2 given by:

$$\begin{aligned}X_1 = \kappa_3[&3\left|A_1^0\right|^5\left(a_1 + a_1^*\right) + 36\left|A_1^0\right|^3\left|A_2^0\right|^2\left(a_2 + a_2^*\right) + 18\left|A_2^0\right|^4 A_1^0\left(a_1 + a_1^*\right)\\ &+12\left|A_1^0\right|^4 A_2^0\left(a_2 + a_2^*\right) + 24\left|A_1^0\right|^3\left|A_2^0\right|^2\left(a_1 + a_1^*\right) + 12\left|A_2^0\right|^5\left(a_2 + a_2^*\right)],\\ X_2 = \kappa_6[&12\left|A_1^0\right|^5\left(a_1 + a_1^*\right) + 24\left|A_2^0\right|^3\left|A_1^0\right|^2\left(a_2 + a_2^*\right) + +12\left|A_2^0\right|^4 A_1^0\left(a_1 + a_1^*\right)\\ &+18\left|A_1^0\right|^4 A_2^0\left(a_2 + a_2^*\right) + 36\left|A_1^0\right|^3\left|A_2^0\right|^2\left(a_1 + a_1^*\right) + 3\left|A_2^0\right|^5\left(a_2 + a_2^*\right)]\end{aligned}$$

where a_j^* is the complex conjugate of a_j. At this step, to study the stability of the above set of linear equations, we used the Fourier and Laplace transform of the perturbation as follows:

$$a_j(z,t) = \frac{1}{\sqrt{2\pi}} \int a^{-ikz} a^{i\Omega t} \hat{a}_j(\Omega,k) dk d\Omega, \tag{13}$$

$$n_j(z,t) = \frac{1}{\sqrt{2\pi}} \int a^{-ikz} a^{i\Omega t} \hat{n}_j(\Omega,k) dk d\Omega, \tag{14}$$

where $\hat{a}_j(\Omega,k)$ and $\hat{n}_j(\Omega,k)$ stands as Fourier transform in time and Laplace transform in space, Ω and k are, respectively, the frequency pump and wave number of perturbation. Putting Eq. (13) in the previous set of equations (Eqs. (9)–(12)) and after eliminating $(\hat{n}_j(\Omega,k))$, we obtain a set of two homogeneous equations for a_1, a_1^*, a_2, and a_2^*. Then by considering their conjugates, we obtain a set of four homogeneous equations. The resulting matrix presents a nontrivial solution only when the dispersion relation satisfies the following relation:

$$\left[\left(k - \frac{\Omega}{v_{g1}}\right)^2 - f_1\right]\left[\left(k - \frac{\Omega}{v_{g2}}\right)^2 - f_2\right] = C_{XPM}, \tag{15}$$

where the parameters of this equation are defined by the following relation:

$$\begin{aligned} f_1 = B_1(\Omega)[B_1(\Omega) &+ 2\tilde{\gamma}_1\kappa_1|A_1^0|^2 + 4\tilde{\gamma}_1\kappa_2\left(|A_1^0|^4 + 3|A_1^0|^2|A_2^0|^2\right) \\ &+6\tilde{\gamma}_1\kappa_3\left(|A_1^0|^6 + 6|A_1^0|^2|A_2^0|^4 + 8|A_1^0|^4|A_2^0|^2\right)], \end{aligned} \tag{16}$$

$$\begin{aligned} f_2 = B_2(\Omega)[B_2(\Omega) &+ 2\tilde{\gamma}_2\kappa_4|A_2^0|^2 + 4\tilde{\gamma}_2\kappa_5\left(|A_2^0|^4 + 3|A_1^0|^2|A_2^0|^2\right) \\ &+6\tilde{\gamma}_1\kappa_6\left(|A_2^0|^6 + 6|A_1^0|^4|A_2^0|^2 + 8|A_1^0|^2|A_2^0|^4\right)] \end{aligned} \tag{17}$$

$$\begin{aligned} C_{XPM} = {} & 16B_1(\Omega)B_2(\Omega)\tilde{\gamma}_1\kappa_1\tilde{\gamma}_2\kappa_4|A_1^0|^2|A_2^0|^2 \\ &+16B_1(\Omega)B_2(\Omega)[9\tilde{\gamma}_1\kappa_2\tilde{\gamma}_2\kappa_5\left(|A_1^0|^2|A_2^0|^6 + |A_1^0|^6|A_2^0|^2 + 2|A_1^0|^4|A_2^0|^4\right) \\ &+3\tilde{\gamma}_1\kappa_1\tilde{\gamma}_2\kappa_5\left(|A_1^0|^2|A_2^0|^4 + |A_1^0|^4|A_2^0|^2\right) + 3\tilde{\gamma}_1\kappa_2\tilde{\gamma}_2\kappa_4\left(|A_1^0|^4|A_2^0|^2 + |A_1^0|^2|A_2^0|^4\right) \\ &+6\tilde{\gamma}_1\kappa_1\tilde{\gamma}_2\kappa_6\left(|A_1^0|^6|A_2^0|^2 + |A_1^0|^2|A_2^0|^6 + 3|A_1^0|^4|A_2^0|^4\right) + 6\tilde{\gamma}_1\kappa_3\tilde{\gamma}_2\kappa_4(|A_1^0|^6|A_2^0|^2 + |A_1^0|^2|A_2^0|^6 \\ &+3|A_1^0|^4|A_2^0|^4) + 18\tilde{\gamma}_2\kappa_2\tilde{\gamma}_2\kappa_6\left(|A_1^0|^8|A_2^0|^2 + |A_1^0|^2|A_2^0|^8 + 4|A_1^0|^4|A_2^0|^6 + 4|A_1^0|^6|A_2^0|^4\right) \\ &+18\tilde{\gamma}_1\kappa_3\tilde{\gamma}_2\kappa_5\left(|A_1^0|^8|A_2^0|^2 + |A_1^0|^2|A_2^0|^8 + 4|A_1^0|^6|A_2^0|^4 + 4|A_1^0|^4|A_2^0|^6\right) \\ &+36\tilde{\gamma}_1\kappa_3\tilde{\gamma}_2\kappa_6\left(6|A_1^0|^8|A_2^0|^4 + 6|A_1^0|^4|A_2^0|^8 + |A_1^0|^{10}|A_2^0|^2 + |A_1^0|^2|A_2^0|^{10} + 11|A_1^0|^6|A_2^0|^6\right)] \end{aligned} \tag{18}$$

With the parameters $B_1(\Omega) = \beta_{21}\frac{\Omega^2}{2} - \beta_{31}\frac{\Omega^3}{6} + \beta_{41}\frac{\Omega^4}{24}$ and $B_2(\Omega) = \beta_{22}\frac{\Omega^2}{2} - \beta_{32}\frac{\Omega^3}{6} + \beta_{42}\frac{\Omega^4}{24}$. Eq. (15) looks similar to the case of dispersion relation obtained from nonlinear Schrödinger equation with second order dispersion. However, the difference here arising from the definition of the parameters f_1, f_2, and C_{XPM}. Hence, the dispersion relation obtained above [Eqs. (15)–(18)] regulates the stability condition for the steady-state solution against harmonic perturbations. This stability condition depends on XPM, HOD, and HON. The perturbations grow exponentially if the wave vector k acquires an imaginary part, along the medium with the MI gain given by the relation $g(\Omega) = 2Im(k)$. Consequently, we can examine qualitatively and quantitatively the role played by the delayed nonlinear response (τ) and the group velocity mismatch (δ).

Hence, for usual Kerr approach ($\tau = 0\,ps$) and for non null XPM ($C_{XPM} \neq 0$), it is straightforward to notice that the dispersion relation is fourth order polynomial with real coefficients in k which yields four solutions. From these four solutions, two are always real and thus, irrelevant to investigations of MI. However, the two other can probably be a complex conjugate pair, thereby could affect the MI dynamics and leading to only one unstable gain sideband in the case of cubic nonlinearity as extensively studied in diverse previous works [8, 20, 29, 33, 34, 36–38]. On the other hand, all the four solutions are complex conjugate pairs as far as higher-order effects are concerned and therefore can participate in the MI dynamics; this feature leads to the possibility of two unstable gain sidebands [9]. As the GVM is defined by $\delta = |v_{g1}^{-1} - v_{g2}^{-1}|$, then while considering that the two optical beams are so close to each other by assuming $v_{g1} \approx v_{g2}$, that is, the GVM is negligible [29], these four solutions are given by:

$$k = \frac{\Omega}{v_{g1}} \pm \frac{1}{2}\sqrt{f_1 + f_2 \pm 2\sqrt{(f_1+f_2)^2 + 4\left(C_{XPM} - f_1 f_2\right)}}, \tag{19}$$

The condition so that MI can occur read as: $C_{XPM} > f_1 f_2$. Thus using Eqs. (16), (17), and (18), this condition reads as:

$$\begin{aligned}
&\left[\frac{B_1(\Omega)}{2\tilde{\gamma}_1\kappa_1|A_1^0|^2} + \sum sgn\left(\beta_{ji}\right) + \frac{2\kappa_2\left(|A_1^0|^2 + 3|A_2^0|^2\right)}{\kappa_1} + \frac{6\kappa_3\left(|A_1^0|^4 + 6|A_2^0|^4 + 8|A_1^0|^2|A_2^0|^2\right)}{\kappa_1}\right] \\
&\times\left[\frac{B_2(\Omega)}{2\tilde{\gamma}_2\kappa_4|A_2^0|^2} + \sum sgn\left(\beta_{ji}\right) + \frac{2\kappa_5\left(3|A_1^0|^2 + |A_2^0|^2\right)}{\kappa_4} + \frac{6\kappa_6\left(6|A_1^0|^4 + |A_2^0|^4 + 8|A_1^0|^2|A_2^0|^2\right)}{\kappa_4}\right] < 4 \\
&+\frac{4}{\kappa_1\kappa_4}\left\{\left(|A_1^0|^2 + |A_2^0|^2\right)\left[9\kappa_2\kappa_5\left(|E_1^0|^2 + |A_2^0|^2\right) + 3(\kappa_1\kappa_5 + \kappa_2\kappa_4)\right] + \left[6(\kappa_1\kappa_6 + \kappa_3\kappa_4)(|A_1^0|^6|A_2^0|^2\right.\right. \\
&+|A_1^0|^2|A_2^0|^6 + 3|A_1^0|^4|A_2^0|^4) + 18(\kappa_2\kappa_6 + \kappa_3\kappa_5)\left(|A_1^0|^8|A_2^0|^2 + |A_1^0|^2|A_2^0|^8 + 4|A_1^0|^4|A_2^0|^6 + 4|A_1^0|^6|A_2^0|^4\right) \\
&\left.\left.+36\kappa_3\kappa_6\left(6|A_1^0|^8|A_2^0|^4 + 6|A_1^0|^4|A_2^0|^8 + |A_1^0|^{10}|A_2^0|^2 + |A_1^0|^2|A_2^0|^{10} + 11|A_1^0|^6|A_2^0|^6\right)\right]\right\}
\end{aligned} \tag{20}$$

This condition shows that MI depends on the sign of β_{ji} and there is a range of frequency (Ω) over which the MI gain can exist. Thus at these frequencies, the steady-state solution becomes unstable to perturbations. Then, irrespective of the sign of dispersion parameters, this condition can lead to instability because of the presence of XPM that enhanced the MI.

By considering the effects of relaxation time ($\tau \neq 0$), from dispersion relation [Eqs. (15)–(18)], one can observe that the terms C_{XPM} and f_j are complex and consequently produce an imaginary part to the wave number k at any frequency, despite the sign of dispersion parameters. The dispersion relation [Eq. (15)] gives rise to fourth-order polynomial equation with complex coefficients for any finite value of delay response time (τ). Due to the fact that the complex roots do not really appear in conjugate pairs, one has the possibility to obtain until four unstable modes for a given frequency Ω [38]. Therefore, the combine effect of relaxation time and XPM gives rise to four unstable modes contrarily to the case of an instantaneous system. Hence, the role of septic nonlinearity inducing MI is illustrated taking into consideration the effects of walk-off and delay response time for the case in which one of the beams is experiencing normal GVD ($\beta_{ij} > 0$) and the other beam undergoes anomalous GVD ($\beta_{21} < 0, \beta_{22} < 0$) as well as mixed GVD ($\beta_{21} < 0, \beta_{22} > 0$) and "total mixed" GVD ($\beta_{i1} < 0, \beta_{i2} > 0$), ($i = 2, 3, 4; j = 1, 2$). We will separately discuss these cases. Firstly, we illustrate directly the effect of septic nonlinearity on MI gain spectrum for low dispersion and discuss the role of walk-off, the delay response time, and the combine effect of these two parameters. Secondly, we investigate the impact of HOD and HON as well as the nonlinear response time on MI gain spectrum. We end our analysis with the investigation of the septic parameters κ_3. In numerical calculation, we use the following value parameters: the nonlinear terms are given by $\gamma_1 = \gamma_2 = 0.015\ W^{-1}m^{-1}$, the dispersion parameters are $\beta_{21} = \beta_{22} = \pm 0.060\ ps^2m^{-1}$, $\beta_{41} = \beta_{42} = \pm 0.00010\ ps^4m^{-1}$, the TOD is giving in the range $\delta_1 = (0 - 8) \times 10^{-4}\ ps^3m^{-1}$, and the input power is given by $\left|E_j^0\right|^2 = 100\ V.m^{-1}$.

3. Effects of weak dispersion on XPM-induced modulation instability

We investigate the effect of HON on MI gain in the case of low dispersion regime ($\beta_{31} = \beta_{32} = \beta_{41} = \beta_{42} = 0$), considering the effects of walk-off, nonlinear response time, and their combination. In this regime, several studies have been conducted and authors have shown the interplay between walk-off and delay response time [8, 9, 13, 34, 38, 39].

3.1 Roles of walk-off and relaxation of nonlinear response on modulation instability gain spectra

First, let us briefly consider the case of instantaneous response time ($\tau = 0$). In this case, Eq. (15) gives rise to four roots as defined by Eq. (19) which turns to two for null GVM ($\delta = 0$) in normal dispersion regime and to one for mixed dispersion regime, while these equations also turn to two for non null GVM and as GVM reaches certain values, these two roots turned to one. This feature is given in **Figure 1(a)** where one can note different MI gain spectra. Obviously, we noted from this figure that, for null GVM in normal and mixed GVD, the behavior of MI

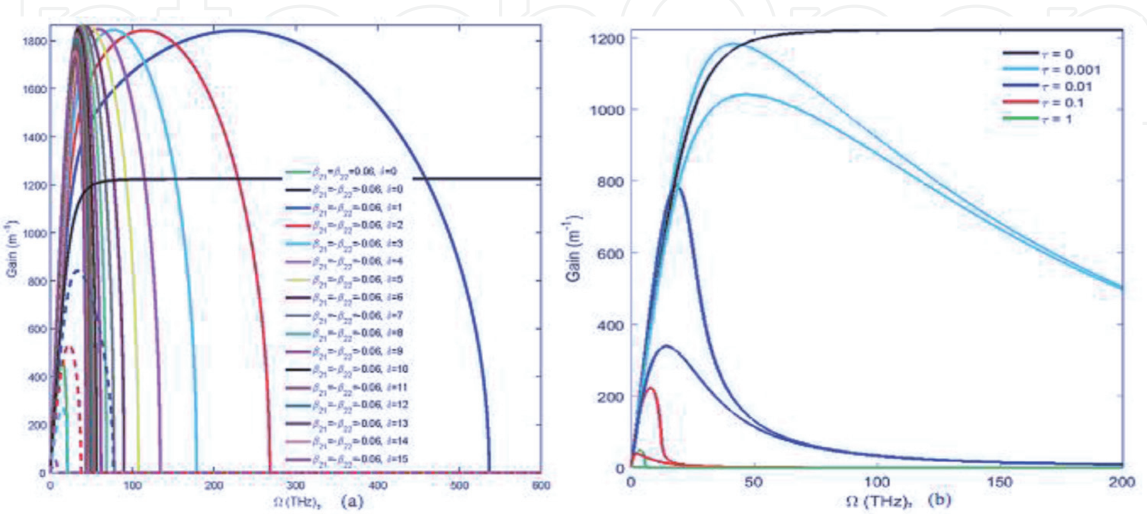

Figure 1.
MI gain spectra $g\ (m^{-1})$ as a function of the frequency Ω (THz): (a) for different value of GVM with $\tau = 0$ and (b) in non-instantaneous response time ($\tau \neq 0$) system with null GVM.

gain spectrum is as described in Ref. [39]. Its mean that, taking into account the effect of GVM, the description remain; however, we showed that, as GVM increases the MI gain increase till reach certain values ($\delta = 7$) and started decrease. We also got two gain maxima for more value of delta than in [39] (see blue to magenta curves). This aspect is due to septic nonlinearity.

Now, considering the effect of delay response time by setting GVM null, Eq. (15) leads to four unstable modes which turns to two as given in **Figure 1(b)**. We note from this figure that, for ultra-fast response time, the behavior is as for fast response time for cubic nonlinearity, and the rest of the curves is as described in quintic nonlinearity [39]. As already mentioned, the non-instantaneous response time brings new bands attributed to Raman effect involves in the fibers.

3.2 Combined effects of walk-off and delay response time on modulation instability gain spectra

Taking into account the combined effects of delay response time and GVM, Eq. (15) leads to four unstable modes that turns to two for response time reaching certain value ($\tau = 1$) and coalesce into one at high frequencies. This is given in **Figure 2** where we have fixed the value of δ and varied the nonlinear response time. For mixed GVD, our results shows that, for fast response time ($\tau = 0.01ps$, see blue curve), the conventional band increases when GVM increases, while the Raman band decreases and their width shift toward lower frequencies. The spectra seem the same as in the case of quintic nonlinearity [39].

Now considering that GVM varies with fixed nonlinear response time, we have observed that when the GVM increases, the behavior of the MI gain spectra changes drastically as given in **Figure 3** for mixed GVD. In this figure, the four unstable modes coalesce into one at high frequencies.

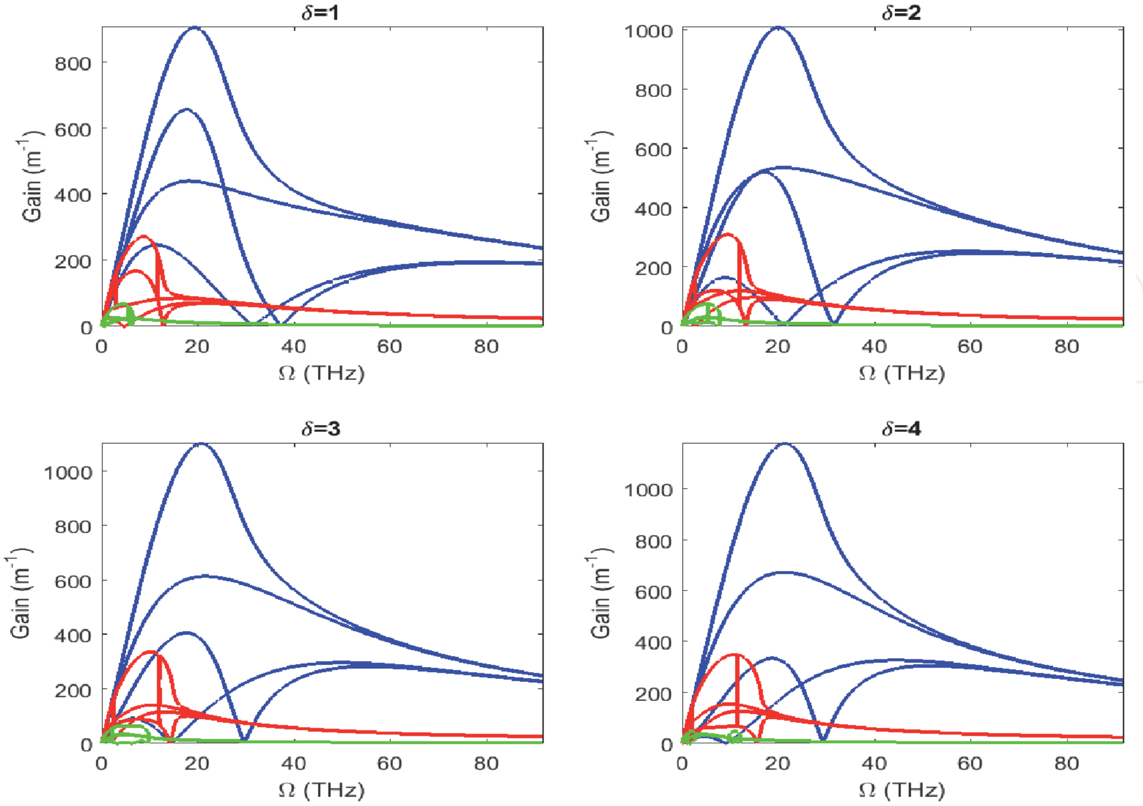

Figure 2.
MI gain spectra g (m^{-1}) as a function of the frequency Ω (THz) for non null GVM and nonlinear response time.

However, for fast response time gives in **Figure 3(a)**, we observe that for conventional and Raman band, the magnitude increases when δ increases; it is the inverse for the sporadic band while their width slightly enlarge and shift toward higher frequencies. The situation is different in the case of slow response time $(\tau = 0.1ps)$ as given in **Figure 3(b)**. We observe that as δ increases, the magnitude of conventional MI gain decreases with the appearance of the Raman peaks that shift toward higher frequencies as GVM increases. The behavior of the Raman band remains as in panel (a). However for the sporadic band, their magnitude increases as δ increases and their width enlarges with the appearance of the sporadic peaks that shift toward higher frequencies. These Raman and sporadic peaks are probably brought by the combined effect of delay response time and opposite sign of SOD.

In the case of anomalous dispersion regime, the four unstable mode turns to two modes as given in **Figure 4**. One can observe from this figure that, for conventional spectral band, as GVM increases, the MI gain decreases, while for Raman band (second spectral band), it is inverted. However, the behavior of the MI gain spectra is different from these panels and we can see that as nonlinear response time increases, the magnitude of the gain decreases. In panel (a), we note that before extended in all frequencies, the curves are neutralized at a given frequency and

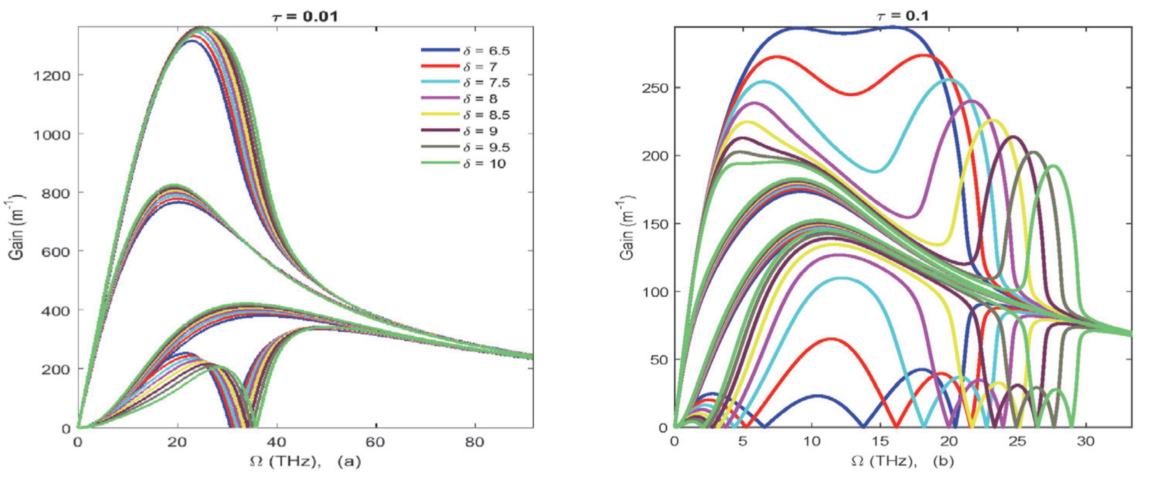

Figure 3.
MI gain spectra g (m^{-1}) as a function of the frequency Ω (THz) for different values of δ in mixed GVD. (a) for τ = 0.01ps, (b) for τ = 0.1ps.

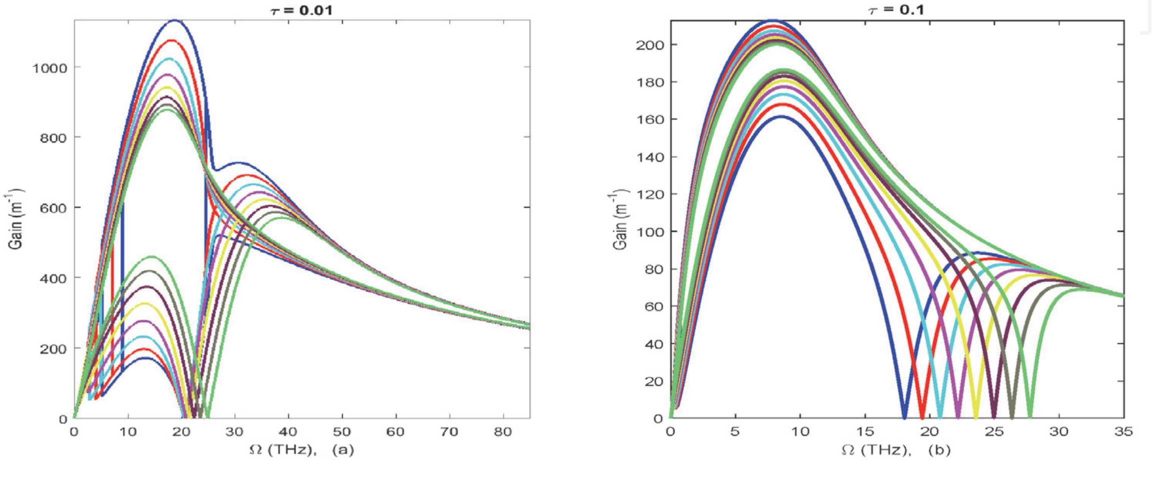

Figure 4.
*MI gain spectra g (m^{-1}) as a function of the frequency Ω (THz) for different values of δ in anomalous GVD. (a) for τ = 0.01ps, (b) for τ = 0.1ps. The colors and the δ values are the same in **Figure 3**.*

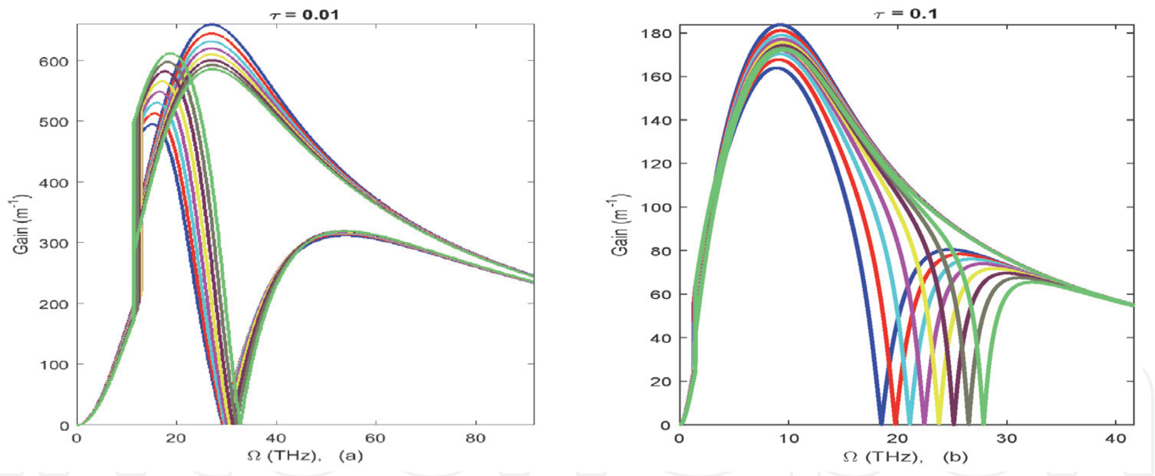

Figure 5.
MI gain spectra g (m^{-1}) as a function of the frequency Ω (THz) for different values of δ in normal GVD. (a) for τ = 0.01ps, (b) for τ = 0.1ps. The colors and the δ values are the same in ***Figure 3****.*

move slowly toward high frequencies while in panel (b), they move rapidly as GVM increases.

In the case of normal dispersion regime, for slow response time [panel (a)], the two unstable modes turn to one for lower frequencies and to two at characteristic frequency until colliding to one at high frequencies. The previous description in anomalous case remains the same. Meanwhile for fast response time [panel (b)], the situation is slightly different where one can observe two unstable modes that collid to one as GVM increases. **Figure 5** portrays this feature. The Raman and sporadic peaks observed previously in **Figure 3** disappeared in these figures due probably to the sign of SOD (they have the same sign).

4. Impact of higher-order dispersion and septic nonlinearity on XPM-induced modulation instability

It has been shown that HOD effects such as FOD and TOD are most essential and give rise to a wide diversity of information concerning the MI dynamics.

4.1 Effect of fourth-order dispersion on modulation instability

The inclusion of FOD brings a great change to the MI spectrum and we obtain for each GVM value four gain spectra. In the case of mixed dispersion regime, from **Figure 6** we note that, the spectrum presents two regions of instability which are connected to each other. The first one at the pump frequency is separated to the second one due to the effect of FOD. Thus in the case of fast delay response time gives in panel (a), one can observe that for the first instability region, the primary band remains unchanged for all GVM values; while for the Raman band as GVM increases, the MI gain spectra increase. For the second instability region, the situation remains the same as in the mixed case for weak dispersion regime (**Figure 3(a)**). In panel (b), our work unveiled that for first instability region, the conventional spectral MI gain decreases as GVM increases, while it is inverted for Raman bands. According to the second instability region, we revealed the presence of Raman and sporadic peaks that magnitude and width decrease as GVM increases and they move toward high frequencies. The fourth unstable mode turns to one at high frequencies. In addition at around $\Omega = 15Thz$, we observe a singularity brought by FOD. In panel (a), this effect neutralized the spectra at this point.

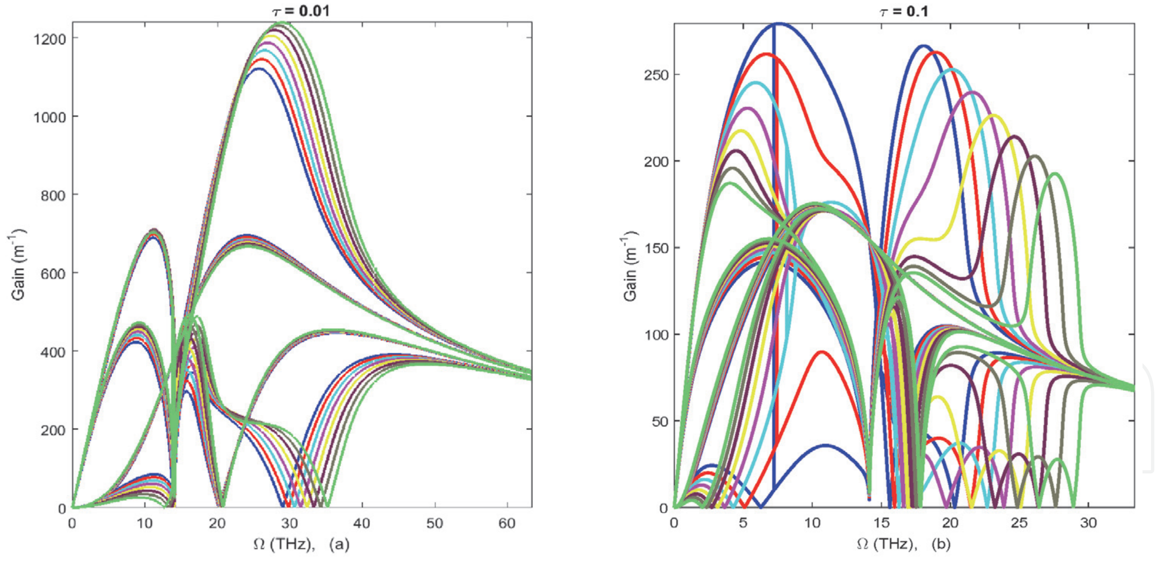

Figure 6.
*MI gain spectra g (m^{-1}) as a function of the frequency Ω (THz) for different values of δ in mixed GVD with the inclusion of FOD. (a) for τ = 0.01ps, (b) for τ = 0.1ps. The colors and the δ values are the same in **Figure 3**.*

Taking into account the propagation with anomalous GVM qualitatively changes the MI spectrum, like shape as in **Figure 7** that for the primary spectral band as GVM increases, the MI gain spectra decrease, contrarily to the Raman bands which increase as GVM increases. In addition, when increasing the delay response time, the magnitude and the width of MI gain spectra decrease considerably with a singularity around $\Omega = 14Thz$ brought by the effect of FOD. Meanwhile in the case of normal GVD as in **Figure 8**, contrarily to what are observed in previous figures, the inclusion of FOD hardly brings any changes to the MI spectrum due mainly to the dominance of normal GVD over FOD. However, the magnitude of the MI gain has considerably increases precisely for the second spectral band.

4.2 Effect of third-order dispersion on modulation instability

We now shift our analysis to the effect of walk-off and delay response time in virtue of TOD. In the case of mixed GVD as seen in **Figure 9**, the spectra hardly

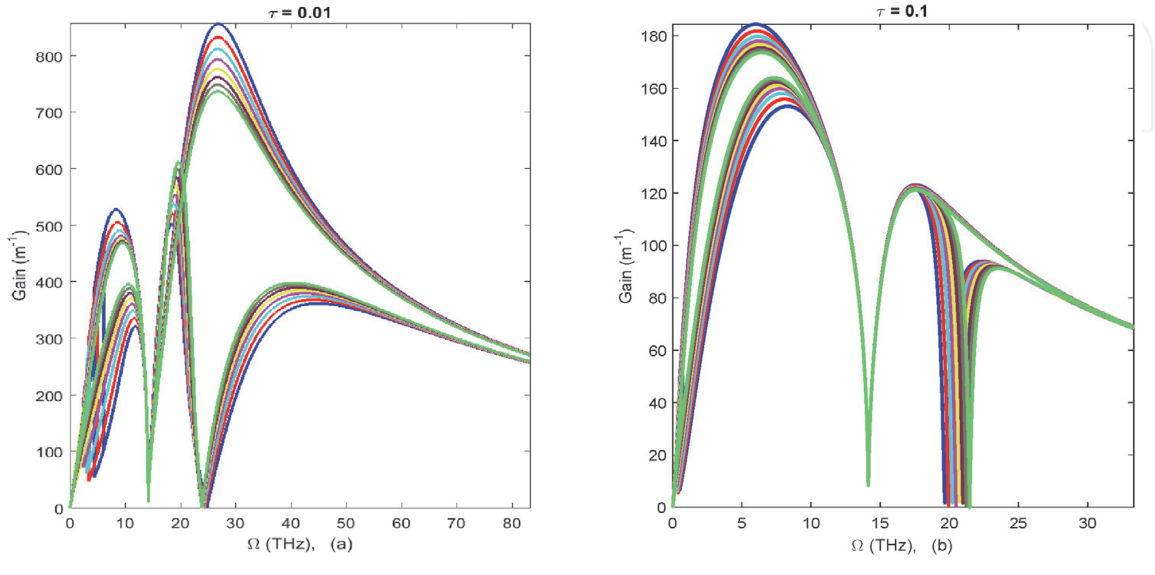

Figure 7.
*MI gain spectra g (m^{-1}) as a function of the frequency Ω (THz) for different values of δ in anomalous GVD with the inclusion of FOD. (a) for τ = 0.01ps, (b) for τ = 0.1ps. The colors and the δ values are the same in **Figure 3**.*

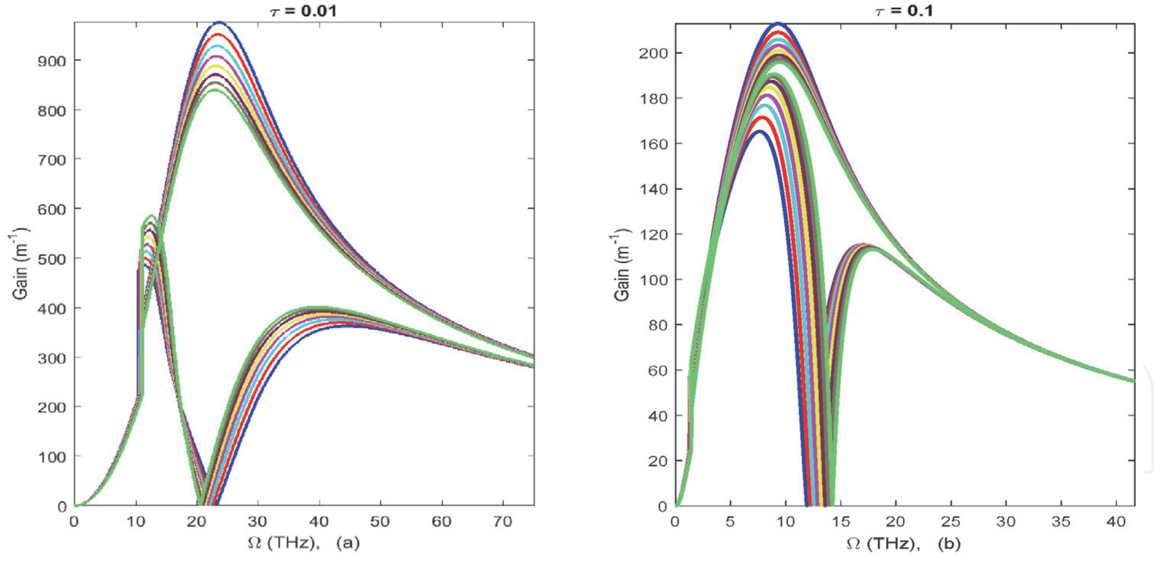

Figure 8.
MI gain spectra g (m^{-1}) as a function of the frequency Ω (THz) for different values of δ in normal GVD with the inclusion of FOD. (a) for τ = 0.01ps, (b) for τ = 0.1ps. The colors and the δ values are the same in ***Figure 3****.*

change for $\tau = 0.01$ [panel (a)] in comparison to **Figure 6** where we considered FOD effect. However, for first instability region, concerning the primary spectral band the magnitude of MI gain slowly increases when GVM increases and their width slightly shifts toward higher frequencies, whereas it is the reverse for second spectral band in this region. In addition, in the case of quintic nonlinearity as done in Ref. [39], the spectrum extended over all frequencies while in this case, we find that the gain spectrum is neutralized three times before extend over all frequencies. The second instability region remains as described in **Figure 6**. Then at high frequencies, the four gain spectra coalesce into one. For slow response time $(\tau = 0.1)$ in panel (b), the first instability region remains unchanged, whereas for the second instability region, we note that as GVM increases, the MI gain spectra increase until it reaches a value $\delta = 8$ before it starts decreasing.

In the case of anomalous dispersion regime, the four obtained solution leads to four unstable modes that coalesce to one at higher frequencies. **Figure 10** depicts

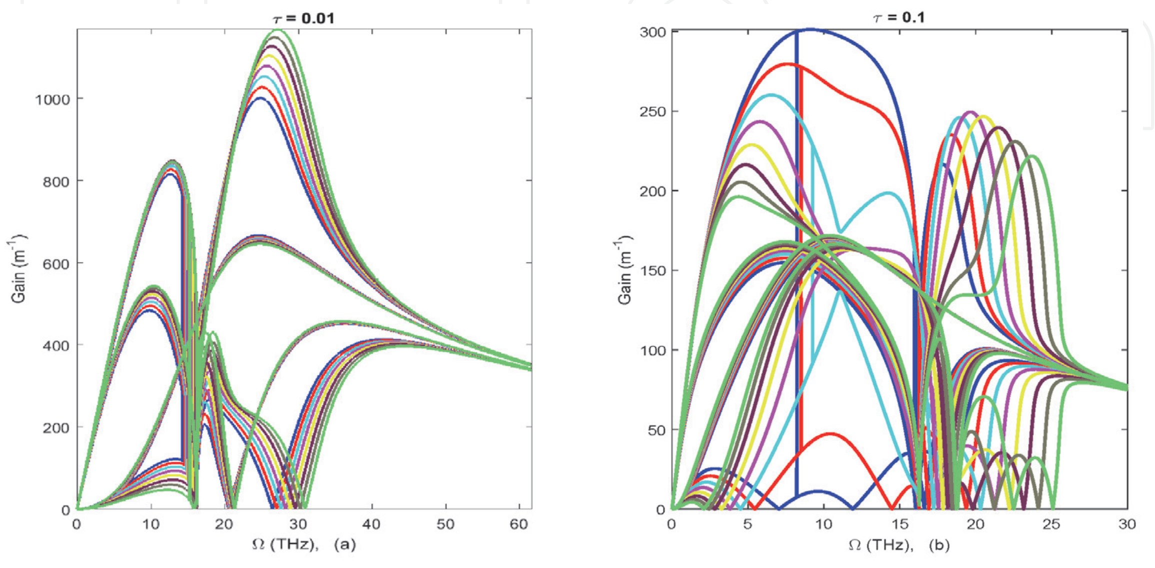

Figure 9.
MI gain spectra g (m^{-1}) as a function of the frequency Ω (THz) for different values of δ in mixed GVD with the inclusion of TOD. (a) for τ = 0.01ps, (b) for τ = 0.1ps. The colors and the δ values are the same in ***Figure 3****.*

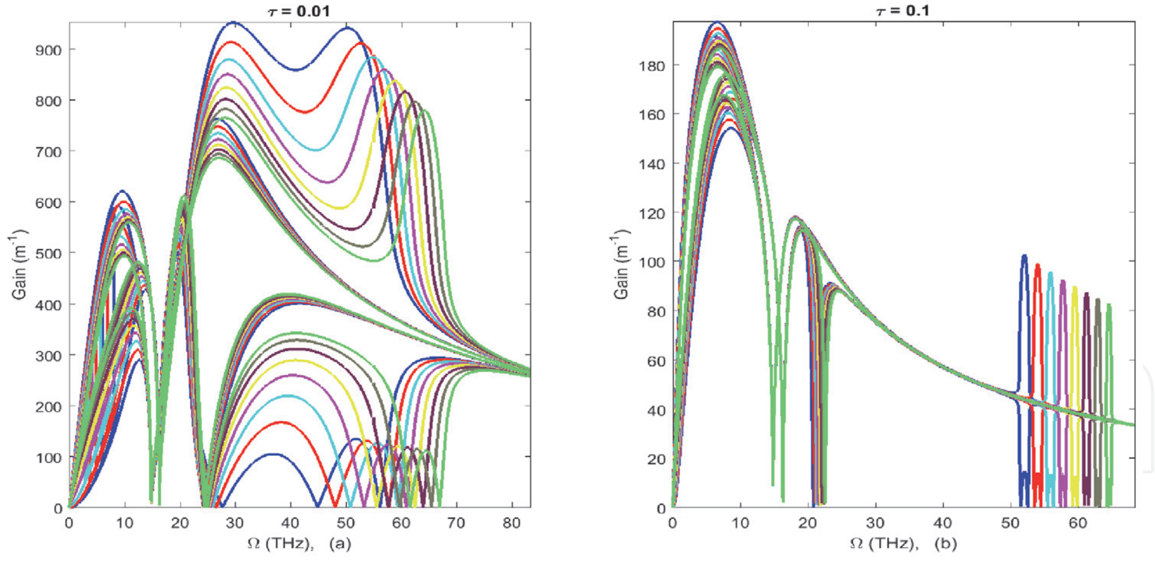

Figure 10.
*MI gain spectra g (m^{-1}) as a function of the frequency Ω (THz) for different values of δ in anomalous GVD with the inclusion of TOD. (a) for τ = 0.01ps, (b) for τ = 0.1ps. The colors and the δ values are the same in **Figure 3**.*

the MI gain spectrum for some GVM value. One observed two singularities due certainly by HOD effects. In the case of fast response time, for first spectral region in panel (a), the primary and Raman bands decrease as GVM increases while for spectra obtained at low MI gain in this region the situation is inverted. In the second region, the inclusion of TOD brings Raman and sporadic peaks that shifted toward higher frequencies due to GVM effect. For slow response time given in panel (b), the situation is almost different as earlier. The sporadic and Raman peaks get shrink and still move toward higher frequencies. It is to explain the behavior of the obtained modes at lower frequencies coalesce to two at middle frequencies and to one at high frequencies. Contrarily to what observed in the case of quintic nonlinearity, in these figures (**Figure 10**), HOD acts in the case of septic nonlinearity.

We now turn our attention to the case of normal dispersion regime as given in **Figure 11**. We note that, the second spectral region remains almost the same as described in previous figure. However, in the first spectral region, the four solution

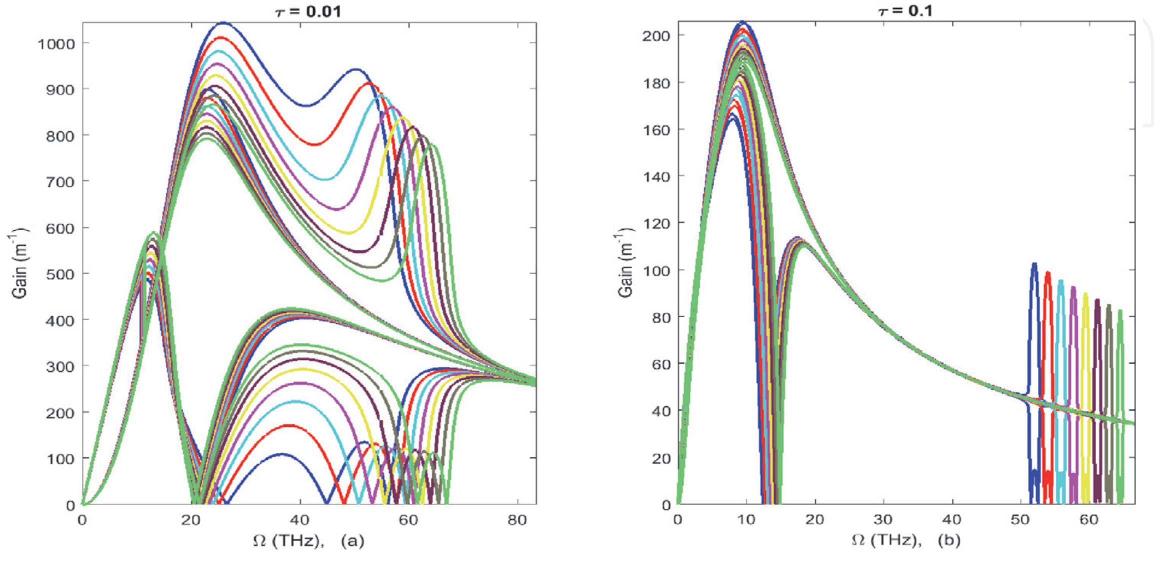

Figure 11.
*MI gain spectra g (m^{-1}) as a function of the frequency Ω (THz) for different values of δ in normal GVD with the inclusion of TOD. (a) for τ = 0.01ps, (b) for τ = 0.1ps. The colors and the δ values are the same in **Figure 3**.*

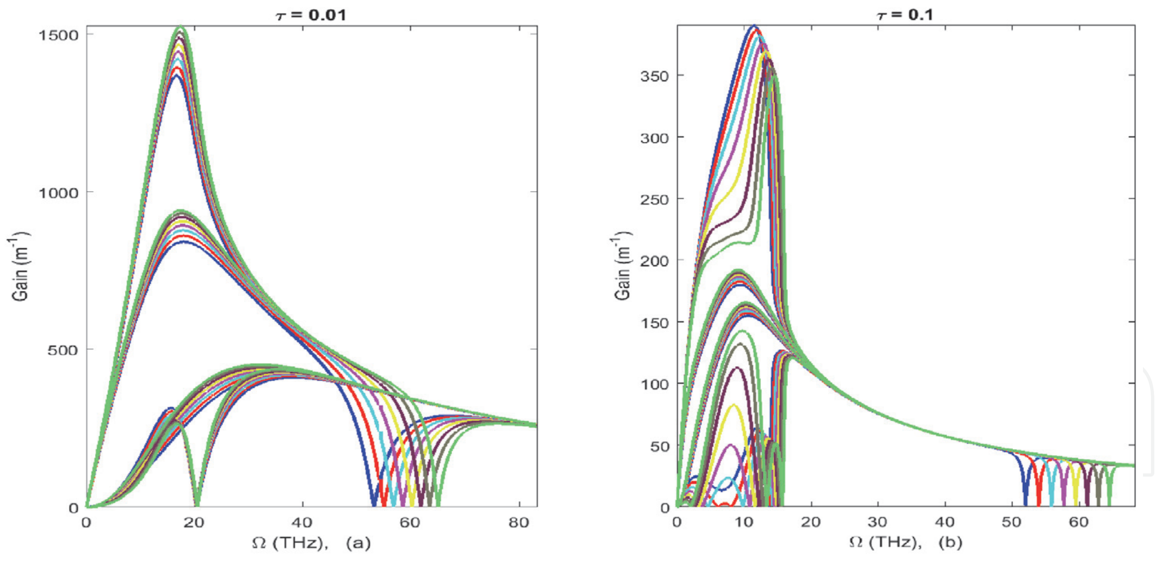

Figure 12.
*MI gain spectra g (m^{-1}) as a function of the frequency Ω (THz) for different values of δ in "total mixed" GVD with the inclusion of TOD. (a) for τ = 0.01ps, (b) for τ = 0.1ps. The colors and the δ values are the same in **Figure 3**.*

leads to two unstable modes in panel (a) and to one in panel (b) for lower frequencies. The effect of FOD vanishes due probably to the dominance of SOD and HON. Obviously, we note that as response time increases, the Raman and sporadic peaks get shrink.

Figure 12 depicts the evolution of MI gain spectra in the case of "total mixed" GVD. It is obvious to see from panel (a) (fast response time) that as GVM increases, the conventional bands decrease while it is inverted for Raman bands. The effects of TOD is visible around $\Omega = 60Thz$ where the spectra are neutralized before extended over all frequencies. According to panel (b) for slow response time, we observe the appearance of Raman peaks in conventional bands brought by the effect of SOD that magnitude decreases as GVM increases and they shifted toward high frequencies however their width get shrink over what observe in **Figure 12(a)**. Also we note the existence of non-conventional bands between $\Omega = (11 - 14)Thz$ due to the effect of FOD that decreases and shift toward high frequencies when GVM increases while is it inverted for the other bands between $\Omega = (2 - 13)Thz$ as the magnitude increases, the width widens toward both the low and high frequencies. The effect of TOD is visible around $\Omega = 60Thz$ with the appearance of singularity. It is important to note from this figure that the Raman peaks observe at higher frequencies in previous figures vanish due probably to the sign of used value.

We generally note from these different figures that, the inclusion of TOD and FOD increases considerably the MI gain spectrum and their width. In addition, the formation of Raman and sporadic peaks observed is due on the one hand to the combined effect of SOD and relaxation time and on the other hand due to the combined effect of TOD. They move toward high frequencies due to the effect of GVM. From fast to slow response time, we note that the magnitude of MI gain spectra decreases considerably. The MI occurs in the case of HOD and septic nonlinearity only when the interactions between beams are less (gives here by walk-off parameter δ).

4.3 Effect of septic nonlinearity parameter κ_3 on modulation instability gain

To better appreciate the effect of septic nonlinearity on MI gain, we portrayed the latter versus κ_6 in different cases above. In other to do this, the solution of Eq. (15) gives rise to four roots that turn to two pairs of roots due to HON effect.

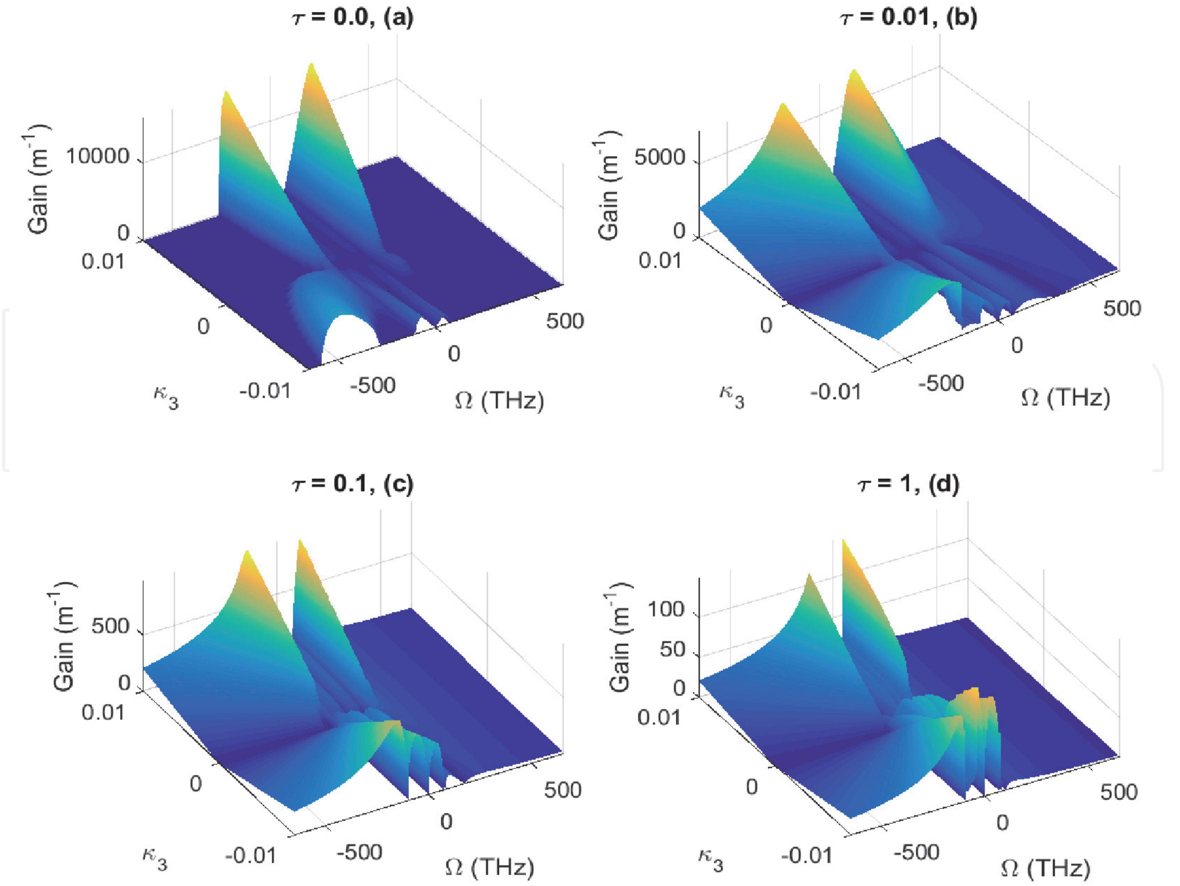

Figure 13.
MI gain spectra g (m^{-1}) as a function of the frequency Ω (THz) and the nonlinear parameter κ_3 in the case of normal GVD for null GVM ($\delta = 0$). (a) τ = 0.0ps, (b) τ = 0.01ps, (c) τ = 0.1ps, (d) τ = 1ps.

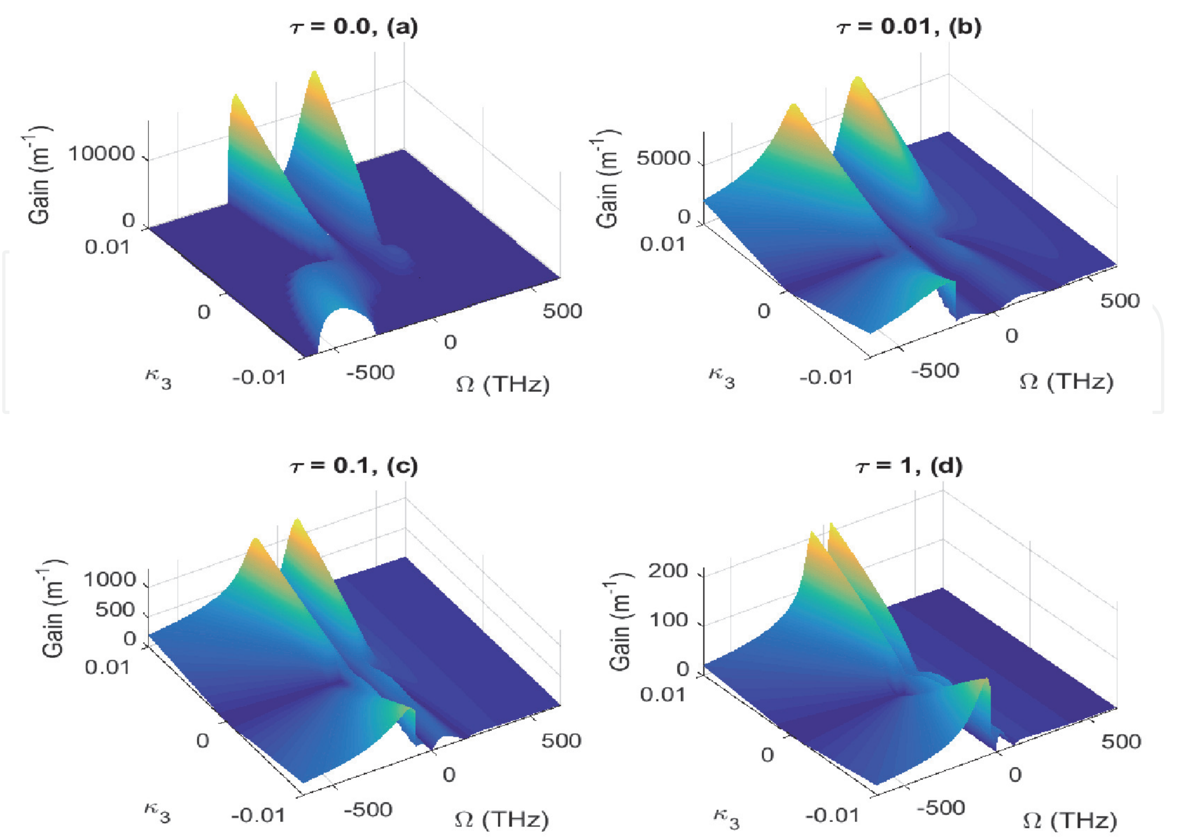

Figure 14.
MI gain spectra g (m^{-1}) as a function of the frequency Ω (THz) and the nonlinear parameter κ_3 in the case of anomalous GVD for null GVM ($\delta = 0$). (a) τ = 0.0ps, (b) τ = 0.01ps, (c) τ = 0.1ps, (d) τ = 1ps.

We have plotted the behavior of the MI gain in **Figure 13** for normal GVD. We observe from this figure that MI appears on both side of κ_3. Each panel shows that the distinct side bands are antisymmetric. As κ_3 increases, the MI gain increases and the bandwidth enlarges. The high value of MI gain is obtained for $\kappa_3 > 0$ and the bandwidth increases when delay response time increases for $\Omega < 0$, while it is inverted for $\Omega > 0$. For instantaneous response time [see panel (a)], we note the appearance of two high side bands for $\kappa_3 > 0$ due to the effect of SOD, while there are three side bands for $\kappa_3 < 0$ brought by TOD around $\Omega = -500$ *Thz* and by FOD around $\Omega = 0$ *Thz* that slowly increases for negative value of κ_3. Considering non-instantaneous response time [see panels (b), (c), and (d)], we note that the side bands are unstable for $\Omega < 0$, while it is slightly unstable for $\Omega > 0$. In addition, as delay response time increases, we note more side bands. The latter information remains in the case of "total mixed" dispersion regime; however, the bandwidth is reversed due probably to opposite signs of the dispersion parameter.

In the case of anomalous dispersion regime plotted in **Figure 14**, we notice that the side bands brought by FOD are suppressed due to their opposite sign with the sign of SOD, the latter dominates and leads to the observed spectrum. Apart from this difference, the information obtained in the normal case remains almost the same. We now turns our attention in the case of mixed dispersion regime gives in **Figure 15**. Our results show that contrarily to what are observed in previous figures, the bandwidth is clearly visible for $\kappa_3 > 0$ where the band rapidly increases as κ increases by enlarging their bandwidth meanwhile for $\kappa_3 < 0$, we notice that the bandwidth progressively appears as delay response time increases. In each panels, the effect of TOD is suppressed due probably to the opposite sign of SOD; this leads to symmetric bandwidth observed. For instantaneous response time in panel (a), the MI gain spectrum appears only for $\kappa_3 < 0$. For non-instantaneous response time,

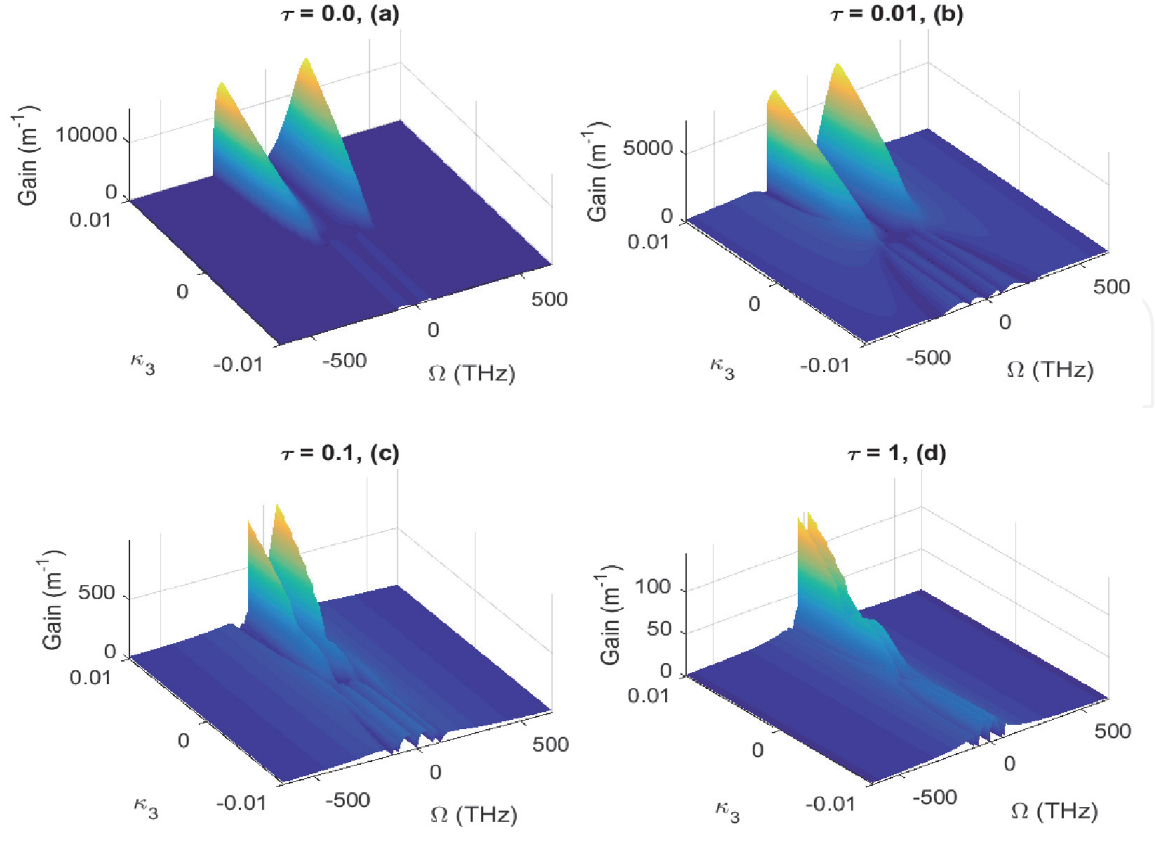

Figure 15.
MI gain spectra g (m^{-1}) as a function of the frequency Ω (THz) and the nonlinear parameter κ_3 in the case of mixed GVD for null GVM ($\delta = 0$). (a) τ = 0.0ps, (b) τ = 0.01ps, (c) τ = 0.1ps, (d) τ = 1ps.

we observe that for $\kappa_3 < 0$, the band slightly appears due to the effect of FOD that bandwidth decreases as delay response time increases.

5. Conclusion

In this work, we have investigated analytically and numerically the MI process in nonlinear Kerr media with delayed Kerr nonlinearity and subjected to XPM, described by a system of two coupled NLS equation with cubic-quintic-septic nonlinearities, experiencing diverse GVD regime. The system is considered by incorporating the Debye relaxational time-dependent nonlinearities in NLS equation with combined high-order effects modeling the propagation of ultrashort optical pulses in highly nonlinear Kerr media. By considering a small harmonic perturbations to the stationary solutions, we derive the exact dispersion relation for the components of the perturbation fields that include both the XPM and relaxation effects. Our study revealed the effects of septic nonlinearity in the case of the pulses co-propagating in diverse GVD regime. Obviously from our work, the incorporation of septic nonlinearity increases considerably the MI gain spectrum with the emergence of new instabilities frequencies contrarily to that was observed in Ref. [8, 9, 38, 39], while the increase of delay response time decreases the magnitude and the width of the MI gain.

Our study unveiled in the case of weak dispersion regime that, in instantaneous Kerr media, the typical frequency converges to finite value for mixed GVD regime with two gain maxima for certain GVM, meanwhile the MI gain continuously grows with the GVM until it reaches certain values before decays. In non-instantaneous Kerr media, we note the appearance of Raman band with the emergence of Raman peaks for slow response time ($\tau = 0.1ps$) in the case of mixed dispersion regime contrarily to what was done in [39]. We note that, these emerged Raman peaks decrease in width and magnitude when the GVM increases and shifts toward higher frequencies.

Now considering the effect of HOD, we observed that their incorporation hardly change the spectrum. The inclusion of FOD does't affect the MI gain in normal dispersion regime contrarily to the works done in the case of cubic and quintic nonlinearities [8, 9, 39] where the effect of FOD vanishes in the case of anomalous GVD. The effects of TOD vanish in the case of mixed dispersion regime. However, in the case of anomalous and normal dispersion regime, we note the appearance of Raman peaks that width and magnitude decrease as GVM increases and get shrink as response time increases. In addition, the four unstable modes observed in fast response time leads to two unstable modes for slow response time. For "total mixed" dispersion regime, we also note the appearance of Raman peaks that slightly shifted toward higher frequencies due to the effects of GVM. The effects of septic nonlinearity was also portrayed and our results unveil the appearance of instability in both side of septic nonlinearity parameter. This aspect shows that MI can be investigated as well as in focusing nonlinearity as in defocusing nonlinearity.

Due to the fact that the MI gain increases when taking into account the effect of HON, we can conclude that the system is more stable against harmonic perturbations. In addition, the incorporation of higher order effects lead to the emergence of Raman peaks on the Raman bands. This means that the incident particles after collision with the molecules of the medium, diffuse with a new energy thus creating the Raman peaks observed resulting to the generation of new frequencies range. The study of MI gain has aroused great enthusiasm within the scientific community, motivated in large part by their potential in innovative applications in information technology and telecommunications.

Author details

Michel-Rostand Soumo Tchio[1*], Saïdou Abdoulkary[2] and Alidou Mohamadou[1,3]

1 Faculty of Sciences, University of Maroua, Maroua, Cameroon

2 Département des SF, Faculté des Mines et des Industries Pétrolieres, Maroua, Cameroon

3 The Abdus Salam International Centre for Theoretical Physics, Trieste, Italy

*Address all correspondence to: rostandsoumotchio@yahoo.fr

References

[1] Bourkoff E, Zhao W, Joseph RI. Evolution of femtosecond pulses in single-mode fibers having higher-order nonlinearity and dispersion. Optics Letters. 1987;**12**:272–274

[2] Abdoulkary S, Aboubakar AD, Aboubakar M, Mohamadou A, Kavitha L. Solitary wave solutions and modulational instability analysis of the nonlinear Schröndinger equation with higher-order nonlinear terms in the left-handed nonlinear transmission lines. Communications in Nonlinear Science and Numerical Simulation. 2015;**22**:1288

[3] Saha M, Sarma AK. Modulation instability in nonlinear metamaterials induced by cubic-quintic nonlinearities and higher order dispersive effects. Optical Communication. 2013;**291**:321–325

[4] Benabid F, Biancalana F, Light PS, Couny F, Luiten A, Roberts PJ, et al. Fourth-order dispersion mediated solitonic radiations in HC-PCF cladding. Optics Letters. 2008;**33**:2680–2682

[5] Tchofo DP, Ngabireng CM, Porsezian K, Kalithasan B. Modulational instability in optical fibers with arbitrary higher-order dispersion and delayed Raman response. Optic Communication. 2006;**266**:142–150

[6] Tchofo DP, Porsezian K. Impact of fourth-order dispersion in the modulational instability spectra of wave propagation in glass fibers with saturable nonlinearity. Journal of the Optical Society of America B. 2010;**27**: 1143–1152

[7] Nithyanandan K, Vasantha Jayakantha Raja R, Uthayakumar T, Porsezian K. Impact of higher-order dispersion in the modulational instability spectrum of a relaxing coupled saturable media. Pramana Journal of Physics. 2014;**82**:339-345

[8] Nithyanandan K, Vasantha Jayakantha Raja R, Porsezian K, Kalithasan B. Modulational instability with higher-order dispersion and walk-off in Kerr media with cross-phase modulation. Physical Review A. 2012; **86**:023827

[9] Soumo Tchio MR, Abdoulkary S, Mohamadou A. Modulation instability induced by high-order dispersion to a coupled nonlinear Schrödinger equation in a single-mode optical fiber with Kerr nonlinearity. Physica Scripta. 2019;**94**: 035207

[10] Chow KW, Wong KKY, Lam K. Modulation instabilities in a system of four coupled nonlinear Schrödinger equations. Physics Letters A. 2008;**372**: 4596–4600

[11] Zhang L, Xiang Y, Dai X, Wen S. Modulation instability in an array of positive- and negative-index waveguides. Journal of the Optical Society of America B. 2014;**31**:3029–3037

[12] Zhong X, Cheng K, Chiang S. Modulation instability with arbitrarily high perturbation frequencies in metamaterials with nonlinear dispersion and saturable nonlinearity. Journal of the Optical Society of America B. 2014; **31**:1484–1493

[13] da Silva GL, Canabarro AA, de Lima Bernardo B. Stochastic noise amplification of partially coherent CW beam in the region of minimum GVD in lossless Kerr media with delayed response. Annals of Physics. 2015;**363**: 476–484

[14] Aitchison JS, Weiner AM, Silberberg Y, Oliver MK, Jackel JL, Leaird DE, et al. Observation of optical solitons in a nonlinear glass waveguide. Optics Letters. 1990;**15**:471–474

[15] Chung Y, Lushnikov PM. Strong collapse turbulence in a quintic nonlinear Schrödinger equation. Physical Review E. 2011;**84**:036602

[16] Reyna AS, de Araújo CB. Spatial phase modulation due to quintic and septic nonlinearities in metal colloids. Optics Express. 2014;**22**:22456–224569

[17] Reyna AS, de Araújo CB. Nonlinearity management of photonic composites and observation of spatial-modulation instability due to quintic nonlinearity. Physical Review A. 2014; **89**:063803

[18] Reyna AS, de Araújo CB. High-order optical nonlinearities in plasmonic nanocomposites-a review. Advances in Optics and Photonics. 2017;**9**:720–761

[19] Benjamin TB, Feir JE. The desintegration of wave trains on deep water. Journal of Fluid Mechanics. 1967; **27**:417–430

[20] Agrawal GP. Nonlinear Fiber Optic. 3rd ed. University of Rochester: John Wiley and Sons, Academic Press; 2001

[21] Xiang Y, Wen S, Dai X, Tang Z, Su W, Fan D. Modulation instability induced by nonlinear dispersion in nonlinear metamaterials. Journal of the Optical Society of America B. 2007;**24**: 3058–3063

[22] Whitham GB. A general approach to linear and non-linear dispersive waves using a Lagrangian. Journal of Fluid Mechanics. 1965;**22**:273–283

[23] Hasegawa A. Theory and computer experiment on self-trapping instability of plasma cyclotron waves. Physics of Fluids. 1972;**15**:870–881

[24] Ostrovsky LA. Propagation of wave packets and space-time self-focusing in a nonlinear. Soviet Physics—JETP. 1968; **24**:797–800

[25] Zakharov VE, Ostrovsky LA. Modulation instability: The beginning. Physica D. 2009;**238**:540–548

[26] Wu B, Niu Q. Landau and dynamical instabilities of the superflow of Bose-Einstein condensates in optical lattices. Physical Review A. 2001;**64**: 061603(R)

[27] Salasnich L, Parola A, Reatto L. Modulational instability and complex dynamics of confined matter-wave solitons. Physical Review Letters. 2003; **91**:080405

[28] Hasegawa A, Brinkman WF. Tunable coherent IR and FIR sources utilizing modulational instability. IEEE Journal of Quantum Electronics. 1980; **16**:694–697

[29] Agrawal GP. Modulation instability induced by cross-phase modulation. Physical Review Letters. 1987;**59**:880–883

[30] Boucon A. Instabilité modulationnelle et génération de supercotinuum en regime d'exitation quasi-continue dans les fibres optiques hautement nonlinéaires et microstructurées [Thesis]. Besançon France: Université de Franche-Comté; 2008

[31] Cavalcanti SB, Cressoni JC, da Cruz HR, Gouveia-Neto AS. Modulation instability in the region of minimum group-velocity dispersion of single-mode optical fibers via an extended nonlinear Schrödinger equation. Physical Review A. 1991;**43**:6162–6165

[32] Wang Y, Cheng Q, Guo J, Wang W. Sonic horizon dynamics for quantum systems with cubic-quintic-septic nonlinearity. AIP Advances. 2019;**9**: 075206

[33] Agrawal GP. Nonlinear Fiber Optics. SanDiego: Academic; 2001

[34] Canabarro AA, Santos B, Gleria I, Lyra ML, Sombra ASB. Interplay of XPM and nonlinear response time in the modulational instability of copropagating optical pulses. Journal of the Optical Society of America B. 2010; **27**:1878–1885

[35] Kumar M, Nithyanandan K, Porsezian K. Influence of spatial delay on the modulational instability in a composite system with a controllable nonlinearity. Physical Review E. 2018; **97**:062208

[36] Zhong X, Xiang A. Cross-phase modulation induced modulation instability in single-mode optical fiber swith saturable nonlinearity. Optical Fiber Technology. 2007;**13**:271–279

[37] Liu X, Haus JW, Shahriar SM. Modulation instability for a relaxational Kerr medium. Optic Communication. 2008;**281**:2907–2912

[38] Canabarro AA, Santos B, de Lima Bernardo B, Moura AL, Soares WC, de Lima E, et al. Modulation instability in noninstantaneous Kerr media with walk-off and cross-phase modulation for mixed group-velocity-dispersion regimes. Physical Review A. 2016;**93**: 023834

[39] Soumo Tchio MR, Abdoulkary S, Mohamadou A. Raman peaks shift due to walk-off in non-instantaneous Kerr media with higher-order effects. Journal of the Optical Society of America B. 2019;**36**:3479–3491